ALMA Detection of Dark Chromospheric Holes in the Quiet Sun

Maria A. Loukitcheva[1,2,3] , Stephen M. White[4] , and Sami K. Solanki[1,5]
[1] Max-Planck-Institut für Sonnensystemforschung, Justus-von-Liebig-Weg 3, D-37077 Göttingen, Germany
[2] Saint Petersburg branch of Special Astrophysical Observatory, Pulkovskoye chaussee 65/1, St. Petersburg 196140, Russia
[3] Saint Petersburg State University, 7/9 Universitetskaya nab., St. Petersburg 199034, Russia
[4] Space Vehicles Directorate, Air Force Research Laboratory, Albuquerque, NM, USA
[5] School of Space Research, Kyung Hee University, Yongin, Gyeonggi 446-701, Republic of Korea

Abstract

We present Atacama Large Millimeter/submillimeter Array (ALMA) observations of a quiet-Sun region at a wavelength of 3 mm, obtained during the first solar ALMA cycle on 2017 April 27, and compare them with available chromospheric observations in the UV and visible as well as with photospheric magnetograms. ALMA images clearly reveal the presence of distinct particularly dark/cool areas in the millimeter maps with temperatures as low as 60% of the normal quiet Sun at 3 mm, which are not seen in the other data. We speculate that ALMA is sensing cool chromospheric gas, whose presence had earlier been inferred from infrared CO spectra.

Key words: Sun: atmosphere – Sun: chromosphere – Sun: radio radiation

1. Introduction

Observations of the quiet Sun at submillimeter and millimeter wavelengths can provide essential diagnostics of the physical conditions in the solar chromosphere (see, e.g., Loukitcheva et al. 2004; da Silva Santos et al. 2018, and references therein). Submillimeter and millimeter continua originate from the low to middle chromosphere and allow a rather straightforward measurement of the gas temperature at these heights, as the radiation at these wavelengths is coupled linearly to the electron temperature owing to its formation in local thermodynamic equilibrium (LTE) and in the Rayleigh–Jeans limit.

Prior to the advent of the Atacama Large Millimeter/submillimeter Array (ALMA, Wootten & Thompson 2009) quiet-Sun observations at these wavelengths were extremely rare due to the poor (from tens of arcseconds to arcminutes) spatial resolution of most instruments operating at submillimeter/millimeter wavelengths. Unique observations with the 10-element Berkeley–Illinois–Maryland Array (BIMA) at 3.5 mm with a resolution of around 10″, reported in White et al. (2006) and Loukitcheva et al. (2009), resulted in the first successful interferometric mapping of chromospheric structure at millimeter wavelengths. Strong morphological similarities between millimeter brightness and chromospheric emissions in the Ca II K line, the far-ultraviolet continuum, and the photospheric magnetic field were found on these spatial scales, at which the chromospheric network can just about be distinguished from the internetwork. However, the spatial resolution and scale coverage of the BIMA interferometer were insufficient to clearly resolve the arcsecond-scale quiet-Sun fine structure and reliably study correlations with the chromospheric features seen in other spectral domains.

In this Letter we present results of ALMA observations of the quiet Sun in conjunction with cotemporal images at UV, EUV, and visible wavelengths from the *Solar Dynamics Observatory* (*SDO*, Pesnell et al. 2012), the *Interface Region Imaging Spectrograph* (*IRIS*, De Pontieu et al. 2014), and the instruments of the Global Oscillation Network Group (GONG), including the Big Bear Solar Observatory (BBSO) and the Cerro Tololo Interamerican Observatory (CTIO) in Chile.

Observational data are summarized in Section 2. In Section 3 we present the results of comparison of the millimeter images with the data from other spectral domains and report the first detection of particular dark (i.e., cool) regions in ALMA images. Results are discussed and conclusions are drawn in Section 4.

2. Data Collection and Reduction

The ALMA interferometric data were acquired on 2017 April 27 in Band 3 (100 GHz, i.e., a wavelength of 3 mm) in configuration C40-3, which included 38 × 12 m antennae and 8 × 7 m antennae. However, 3 × 12 m and 1 × 7 m antennae failed in calibration, leaving 42 antennae for imaging. A single quiet-Sun target about 200″ southwest of disk center, tracked for solar rotation, was observed in 10.5 minute scans separated by 2 minute calibration scans, with 2 s integrations, for a total of 37 minutes. The Sun was observed for the time interval 16:00–16:45 UT (45 minutes). Interferometric data were supplemented by single-dish images of the full Sun with a cadence of ≈10 minutes, made with ALMA's total power antennae at a resolution of 60″. Individual 2 s interferometric images were mapped and self-calibrated using standard CASA software, then restored with a synthesized beam of 1″.6 and corrected for the primary beam response. The four 2 GHz-wide spectral windows at 93, 95, 105, and 107 GHz were combined in the mapping, as the resulting u, v-coverage was found to improve the images. The mapped field of view (FOV) was about 120″, in order to accommodate the fact that the 7 m dishes have a primary beam (FWHM) of 100″, while the 12 m dishes have an FWHM of 58″ at 100 GHz. The images were made 401 pixels square, with a cell size of 0″.3 and a cadence of 2 s. The final data cube $T_b(x, y, t)$ contains 1090 images. Solar observing with ALMA is described in the commissioning papers by Shimojo et al. (2017) and White et al. (2017), and calibrations followed the prescriptions given therein: in particular, the interferometric images were converted from flux to brightness temperature, and then 7236 K (derived from the target location in the single-dish images) was added to each image to account for the fact that the interferometer resolves out large spatial scales.

Cotemporal data at other wavelengths used in this study comprised 60 photospheric magnetograms with a 45 s cadence from the Helioseismic and Magnetic Imager (HMI, Scherrer et al. 2012) on board the *SDO*, 220 images at 1600, 1700, and 304 Å, obtained with a 12 s cadence by the Atmospheric Imaging Assembly (AIA, Lemen et al. 2012) on board the *SDO*, and 82 *IRIS* slit-jaw images with a 32 s cadence in the 2796 Å Mg II k line. The data series was completed with full-disk images in Hα: 38 images from the BBSO and 35 images from the GONG telescope at CTIO, both taken with a 0.5 Å–0.6 Å bandpass at a 1 minute cadence and a nominal resolution of 2″.

The full-disk *SDO* images were chosen as the coordinate reference against which all other images were coaligned by cross-correlating images averaged over 45 minutes. The remaining image displacements are less than 1″ and do not affect the results of the analysis presented here. The data from the different instruments were analyzed at their original spatial resolution and in their original data format (data numbers, or DN), except for the ALMA data, which were translated into absolute brightness or temperature values (Kelvin) as described above.

3. Results

3.1. Time-averaged Images

For morphological comparison of the chromospheric features seen in different spectral domains we utilized mean images, obtained by averaging in time over the whole observing period. In this way we avoid biasing our results due to very short-lived features. Figure 1 depicts the time-averaged quiet solar chromosphere at different heights from the temperature minimum region (*SDO*/AIA 1600 Å) through the middle chromosphere (*IRIS* 2796 Å Mg II k line and ALMA Band 3) to the upper chromosphere (CTIO Hα) and the transition region (*SDO*/AIA 304 Å), as well as the corresponding *SDO*/HMI line-of-sight photospheric magnetogram. In the time-averaged Band 3 image the brightness range is from 5630 to 9140 K. The time-averaged magnetogram values are within the range of [−70, 540] G.

A bright network is the most prominent feature in all time-averaged images in Figure 1. Enhanced Band 3 emission, shaped like a "seahorse" formed by the six brightness contours between 7500 and 8900 K in Figure 1, coincides with enhanced magnetic flux and increased brightness in other panels, and outlines bright chromospheric network patches. The presence of a particularly dark (cool) area to the right of the ALMA image center is striking (outlined by red contours at 6000 and 6500 K, and located within a blue rectangle in Figure 1(a)), as it is not distinguishable in the UV channels or in the magnetogram. Hereafter, we refer to this dark area as a CHromospheric ALMA Hole (ChAH), as it is apparent only in ALMA images. To study the ChAH phenomenon, we complemented it with three other regions of the same size in the FOV, representing a chromospheric network (black rectangle in Figure 1(a)) and two regions of "average brightness" corresponding to a "normal internetwork" (green and magenta rectangles in Figure 1(a)), and compared observational data for these four regions of interest at different wavelengths. The results of this comparison for data sequences (in the form of histograms) and for images integrated over the
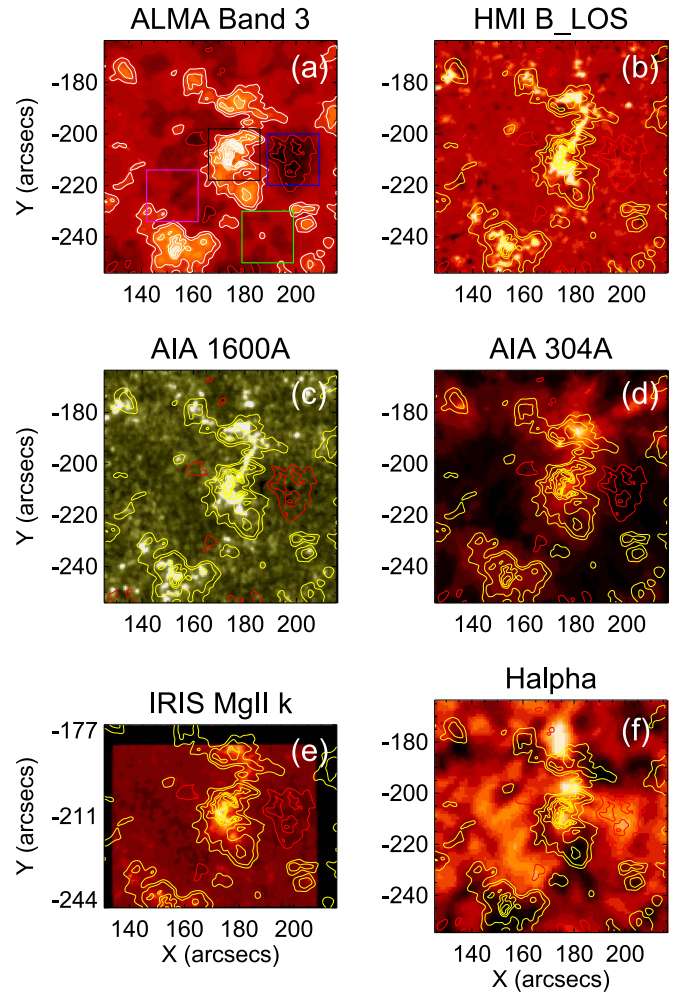

Figure 1. The analyzed quiet-Sun region: (a) ALMA Band 3 ($\lambda \approx 3$ mm) image; (b) *SDO*/HMI magnetogram saturated outside the range [−50, 50]G; (c) and (d) *SDO*/AIA images in the 1600 Å and He II 304 Å channels; (e) *IRIS* Mg II k 2796 Å image; and (f) CTIO Hα image. The AIA images are clipped at 50% of maximum brightness. The overlaid color contours indicate ALMA brightness temperatures at 7500, 7800, 8300, 8500, 8700, and 8900 K (yellow), and at 6000 and 6500 K (red). All images are averaged over 45 minutes. The color rectangles in panel (a) indicate the subregions of interest: a dark region D (blue), a bright network region NW (black), and two internetwork regions, IN1 (magenta) and IN2 (green). The display range of the ALMA image is from 5500 to 9000 K.

full sequence duration are shown in Figures 2–3, and are discussed in the following subsections.

3.2. Time Sequences of Images

In the full ALMA data cube $T_b(x, y, t)$ the brightness range is from 4370 to 11170 K, with the coolest gas being found within the ChAH. Locations in the ChAH region exhibit localized brightness changes with time, but typically only over a range of about 1000 K. In 57% of the 2 s frames there are regions within the blue ChAH rectangle where the brightness temperature is below 5000 K. In general the ChAH remains quite stable over the whole time series, demonstrating that it is a long-lasting phenomenon that is not related to dynamic effects.

To confirm the ChAH's stability over the duration of the observations and to study whether the ChAH differs from the other selected regions of interest at any of the considered wavelengths, we constructed brightness and data number
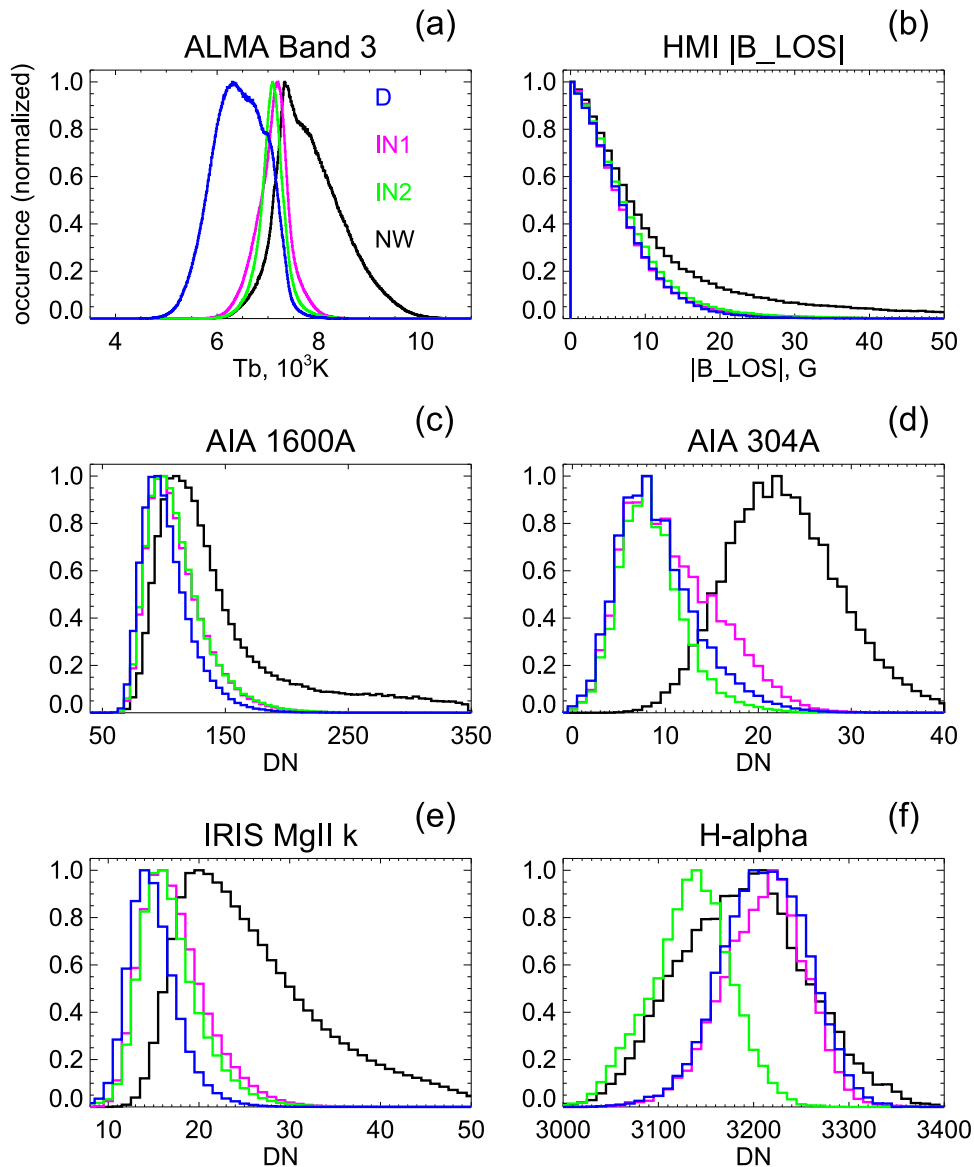
Figure 2. Intensity histograms for the pixels in the four colored squares in Figure 1, with each histogram covering the full cube of (a) ALMA Band 3 (3 mm) data, (b) *SDO*/HMI magnetograms, (c) and (d) *SDO*/AIA images in the 1600 and 304 Å channels, (e) *IRIS* 2796 Å Mg II k images, and (f) CTIO Hα images. The color coding corresponds to that in Figure 1.

histograms. The histograms built from the full time sequence of images at six wavelengths are shown in Figure 2. The dark ChAH region, marked as "D," is plotted in blue, normal internetwork regions ("IN1" and "IN2") are in magenta and in green, respectively, and the chromospheric network patch ("NW") is in black.

The distribution of ALMA brightness (Figure 2(a)) is significantly different from the other wavelengths. The *SDO* and *IRIS* data cubes used here are characterized by distributions with a pronounced high-intensity tail, resembling a log-normal, which is expected for histograms of EUV and UV intensities with sufficiently good statistics (Pauluhn et al. 2000). Band 3 brightness histograms, on the contrary, are largely symmetric. Similar symmetric forms of the ALMA brightness at a shorter wavelength of 1.3 mm were found by Jafarzadeh et al. (2019), while a histogram with a pronounced high-temperature tail was obtained in Loukitcheva et al. (2009) from quiet-Sun BIMA brightness at 3 mm.

Some asymmetry can be seen in the Band 3 histogram for the NW region (black curve in Figure 2(a)), which has more pixels in the high-temperature part, mainly due to magnetic features. Surprisingly, regions with "average" brightness, IN1 and IN2, show narrow and symmetric distributions, with no clear signatures of shocks. The ChAH region (D) has a significantly wider histogram in Band 3 with the histogram maximum located about 1000 K below those of the histograms of the other regions. It is striking that this significant difference between the ChAH and internetwork intensity distributions is seen only at millimeter wavelengths; in the other spectral channels the ChAH histograms are similar to those of the IN1 and IN2 regions, except in the magnesium line (Figure 2(e)). There the ChAH histogram is slightly narrower due to the lack of bright points as compared to IN1 and IN2, but is not clearly offset as in the ALMA data. In Hα, the intensity distributions in D, IN1, and NW are similar to a large extent. Consequently, the ChAH, discovered in the ALMA Band 3
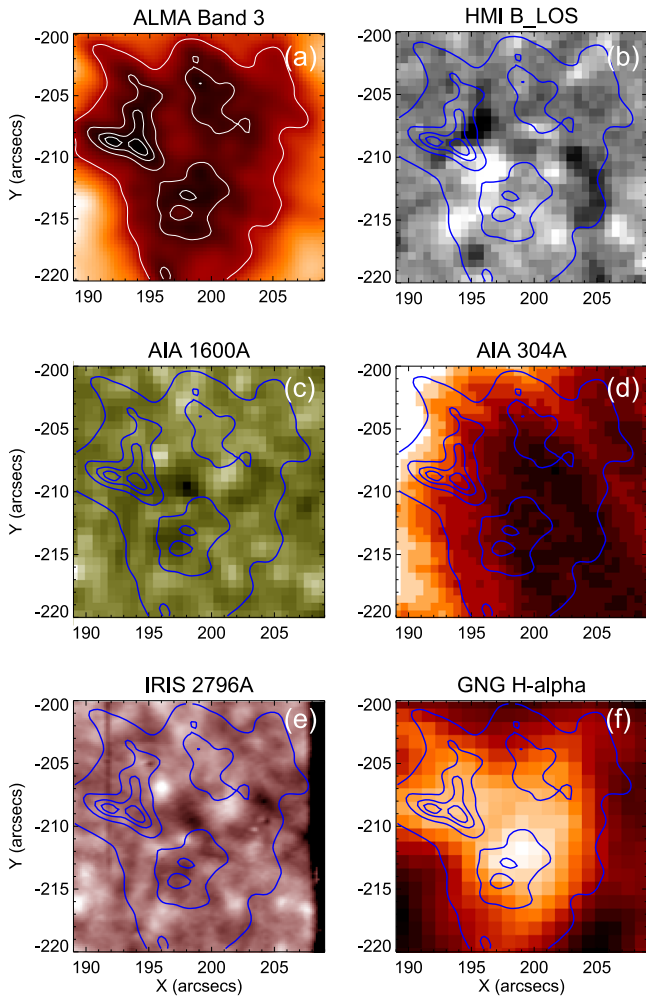
Figure 3. Time-averaged ChAH images at six wavelengths: (a) ALMA Band 3, (b) photospheric magnetogram saturated outside the range [−10,10]G, (c) and (d) AIA channels at 1600 Å and 304 Å, respectively, (e) Mg II k 2796 Å, and (f) Hα. The overlaid color contours indicate ALMA brightness temperatures at 5700, 5800, 6000, and 6500 K. The plotted FOV corresponds to the blue rectangle in Figure 1.

data, is indistinguishable in the full-cube intensity histograms of all the other wavelengths considered.

3.3. Chromospheric ALMA Hole

Figure 3 depicts time-averaged ChAH images at six wavelengths. With horizontal dimensions of approx. $20'' \times 20''$ the ChAH is intermediate in size, between the meso- and supergranule size scales. The brightness temperature ranges from 5600 to 7500 K in the Band 3 image shown in Figure 3(a), while in the ChAH data cube it drops as low as 4370 K, which is about 60% of the quiet-Sun brightness temperature at this wavelength (White et al. 2017). The magnetogram signal in the area is weak, staying within the [−110, 78] G range in the full time sequence. According to Figure 2(b) the ChAH is associated with a similar amount of magnetic field as found in normal internetwork areas. Magnetic concentrations do not appear to avoid the ChAH (Figure 3(b)), unlike the interiors of mesogranular structures (Yelles Chaouche et al. 2011). Nor does it seem to be related to the "dead calm" magnetic areas studied by Martínez González et al. (2012) and characterized by the near absence of magnetic

bipoles. As can be seen from the overlays of millimeter contours in Figure 3 there is no one-to-one correspondence between the localized depressions in Band 3 brightness and the distribution of flux in the UV images. The AIA 304 Å channel also displays a low brightness in this region (Figure 3(d)), although it is not lower than in other IN regions (Figure 2(d)); in Hα the ChAH region, it is relatively bright (Figure 3(f)).

4. Discussion and Conclusions

ALMA data not only distinguish clearly between the network and internetwork; they also show regions that are particularly dark, which we call Chromospheric ALMA Holes (ChAH). Comparing the Band 3 data with those in six wavelengths, covering the full range of chromospheric heights from the temperature minimum to the bottom of the transition region, we conclude that no other data set shows even nearly as clear a difference between ChAH and the normal internetwork as ALMA does. In the Mg II k line, at 304, 1600, and 1700 Å the ChAH region looks equally as dark as normal IN. In the ALMA data, on the contrary, the minimum intensity in the ChAH region (4370 K) is well below the values in other pixels. Hα images look significantly different than Band 3 or any of the other data considered in this work. The fact that the ChAH region is bright in Hα implies that Hα and Band 3 sense different parts of the chromosphere.

In this Letter we have demonstrated that ALMA detects chromospheric features missed by the *SDO* and *IRIS*. For the *SDO* this is not surprising, as in the quiet Sun the HMI line Fe I 6173 Å, and the AIA 1600 and 1700 Å are mainly formed at heights considerably below ALMA Band 3, while 304 Å is formed considerably above, so the *SDO* samples different heights (and temperatures) than ALMA's Band 3 does. Also, the Lyman continuum absorbs any photons emitted by He II 304 Å in the chromosphere, so this line is insensitive to this layer. Similarly, Hα typically forms high in the chromosphere, and responds to any hot gas present there, but is not expected to have much contribution from cool gas because of a lack of excitation of its ground level, $n = 2$. Mg II k-line images are more relevant for a comparison with the Band 3 data, as the radiation at these wavelengths is believed to be formed over similar ranges of heights (e.g., da Silva Santos et al. 2018) and the strength of the central reversal of the line core is thought to follow the temperature quite closely (although extremely nonlinearly; see, e.g., Leenaarts et al. 2013). However, because the core of this line follows temperature exponentially (in the Wien limit), it is expected to be extremely insensitive to cool gas, which is found in the ChAH. The unexpectedly symmetrical form of the Band 3 brightness histograms, in contrast to the roughly log-normal shape of the UV radiation histograms, could be due to the linear relation between gas temperature and brightness at millimeter wavelengths, in contrast to the highly nonlinear relationship in the UV noted above.

It appears that ALMA, through its very unique sensitivity to temperature, has sensed cool chromospheric gas, which has escaped other diagnostics at shorter wavelengths. Thus, the ALMA observations presented here have confirmed that the millimeter continuum is a unique thermal diagnostic for the middle chromosphere. The detection of such low temperatures in ALMA images demonstrates ALMA's potential to differentiate between cool and very cool parts of the chromosphere, which the UV lines cannot do. In UV observations, scattered

light is a significant problem and the excess radiation from some parts of the chromosphere can leak into darker regions due to the huge brightness contrasts. Also, the UV lines pick up the brightest plasma along the LOS and may not be able access the coolest features (e.g., Carlsson & Stein 1995). The presence of very cool gas has been proposed by, e.g., Ayres (1981, 2002), Ayres et al. (1986), and Solanki et al. (1994), based on observations of fundamental-band vibration–rotation transitions of CO in the infrared. The ALMA observations return higher minimum temperatures than those inferred from CO lines. This has two possible causes. First, ALMA Band 3 is formed in the middle chromosphere (Loukitcheva et al. 2004, 2017), while the CO lines mainly sample deeper layers (e.g., Penn 2014). Second, it has to do with the fact that ALMA reacts linearly to temperature, while the CO fundamental-band lines increase nonlinearly in strength with decreasing temperature. Therefore, we expect that in an inhomogeneous atmosphere with hotter and cooler gas along the LOS, the ALMA observations will find temperatures in between those found from CO lines and atomic UV lines. A study of the quiet Sun that is similar to our work but includes ALMA Bands 6 and 7, which sample deeper layers of the chromosphere, and CO lines, would be of considerable value.

ORCID iDs

Maria A. Loukitcheva ⓘ https://orcid.org/0000-0001-5246-9044
Stephen M. White ⓘ https://orcid.org/0000-0002-8574-8629

References

Ayres, T. R. 1981, ApJ, 244, 1064
Ayres, T. R. 2002, ApJ, 575, 1104
Ayres, T. R., Testerman, L., & Brault, J. W. 1986, ApJ, 304, 542
Carlsson, M., & Stein, R. F. 1995, ApJL, 440, L29
da Silva Santos, J. M., de la Cruz Rodríguez, J., & Leenaarts, J. 2018, A&A, 620, A124
De Pontieu, B., Title, A. M., Lemen, J. R., et al. 2014, SoPh, 289, 2733
Jafarzadeh, S., Wedemeyer, S., Szydlarski, M., et al. 2019, A&A, 622, A150
Leenaarts, J., Pereira, T. M. D., Carlsson, M., Uitenbroek, H., & De Pontieu, B. 2013, ApJ, 772, 90
Lemen, J. R., Title, A. M., Akin, D. J., et al. 2012, SoPh, 275, 17
Loukitcheva, M., Solanki, S. K., Carlsson, M., & Stein, R. F. 2004, A&A, 419, 747
Loukitcheva, M., Solanki, S. K., & White, S. M. 2009, A&A, 497, 273
Loukitcheva, M., White, S. M., Solanki, S. K., Fleishman, G. D., & Carlsson, M. 2017, A&A, 601, A43
Martínez González, M. J., Manso Sainz, R., Asensio Ramos, A., & Hijano, E. 2012, ApJ, 755, 175
Pauluhn, A., Solanki, S. K., Rüedi, I., Landi, E., & Schühle, U. 2000, A&A, 362, 737
Penn, M. J. 2014, LRSP, 11, 2
Pesnell, W. D., Thompson, B. J., & Chamberlin, P. C. 2012, SoPh, 275, 3
Scherrer, P. H., Schou, J., Bush, R. I., et al. 2012, SoPh, 275, 207
Shimojo, M., Bastian, T. S., Hales, A. S., et al. 2017, SoPh, 292, 87
Solanki, S. K., Livingston, W., & Ayres, T. 1994, Sci, 263, 64
White, S. M., Iwai, K., Phillips, N. M., et al. 2017, SoPh, 292, 88
White, S. M., Loukitcheva, M., & Solanki, S. K. 2006, A&A, 456, 697
Wootten, A., & Thompson, A. R. 2009, IEEEP, 97, 1463
Yelles Chaouche, L., Moreno-Insertis, F., Martínez Pillet, V., et al. 2011, ApJL, 727, L30